tvst

DOI: 10.1167/tvst.4.4.8

Article

Simulations of Porcine Eye Exposure to Primary Blast Insult

Richard Watson[1,2], Walt Gray[3], William E. Sponsel[1,4,5], Brian J. Lund[6], Randolph D. Glickman[7], Sylvia L. Groth[8], and Matthew A. Reilly[1]

[1] Department of Biomedical Engineering, University of Texas at San Antonio, San Antonio, TX, USA
[2] Biodynamic Research Corporation, San Antonio, TX, USA
[3] Department of Geological Sciences, University of Texas at San Antonio, San Antonio, TX, USA
[4] WESMD Professional Associates, San Antonio, TX, USA
[5] Rosenberg School of Optometry, University of the Incarnate Word, San Antonio, TX, USA
[6] U.S. Army Institute of Surgical Research, JBSA Fort Sam Houston, San Antonio, TX, USA
[7] Department of Ophthalmology, University of Texas Health Science Center, San Antonio, TX, USA
[8] Department of Ophthalmology, University of North Carolina School of Medicine, Chapel Hill, NC, USA

Correspondence: Matthew A. Reilly, 1 UTSA Circle, San Antonio, TX, 78249; e-mail: Matthew.reilly@utsa.edu

Received: 30 March 2015
Accepted: 7 July 2015
Published: 25 August 2015

Keywords: primary blast; ocular trauma; computational modeling; injury modeling; simulation

Citation: Watson R, Gray W, Sponsel WE, et al. Simulations of porcine eye exposure to primary blast insult. 2015;4(4):8, doi:10.1167/tvst.4.4.8

Purpose: A computational model of the porcine eye was developed to simulate primary blast exposure. This model facilitates understanding of blast-induced injury mechanisms.

Methods: A computational model of the porcine eye was used to simulate the effects of primary blast loading for comparison with experimental findings from shock tube experiments. The eye model was exposed to overpressure-time histories measured during physical experiments. Deformations and mechanical stresses within various ocular tissues were then examined for correlation with pathological findings in the experiments.

Results: Stresses and strains experienced in the eye during a primary blast event increase as the severity of the blast exposure increases. Peak stresses in the model occurred in locations in which damage was most often observed in the physical experiments.

Conclusions: Blast injuries to the anterior chamber may be due to inertial displacement of the lens and ciliary body while posterior damage may arise due to contrecoup interactions of the vitreous and retina. Correlation of modeling predictions with physical experiments lends confidence that the model accurately represents the conditions found in the physical experiments.

Translational Relevance: This computational model offers insights into the mechanisms of ocular injuries arising due to primary blast and may be used to simulate the effects of new protective eyewear designs.

Introduction

Ocular trauma has steadily increased as a percentage of overall battlefield injuries, increasing from 0.6% in the Civil War to 13% of all injuries in the Iraq/Afghanistan conflicts as of 2009 (Fig. 1).[1–5] This trend is in agreement with studies done by the military services of other nations over the same time period.[6] Factors affecting this trend are the increased protection of other parts of the body, increased use of fragmentation weapons in general, and increased use of explosive type weapons in particular, such as the improvised explosive devices (IEDs) used by opposing forces in modern day asymmetrical warfare.

Case studies of eye injury in combat generally do not report the mechanism of eye injury. It is therefore difficult to determine which injuries are due to blast alone and which are due to damage from blast-propelled foreign objects.[7] Certainly, the presence of a foreign body in the eye is likely to obscure ocular injuries due to the primary blast alone and would take precedence in the case studies that describe traumatic eye injury in combat. Still, eyes exposed to secondary injury would necessarily also be exposed to primary blast insult though the converse is not necessarily

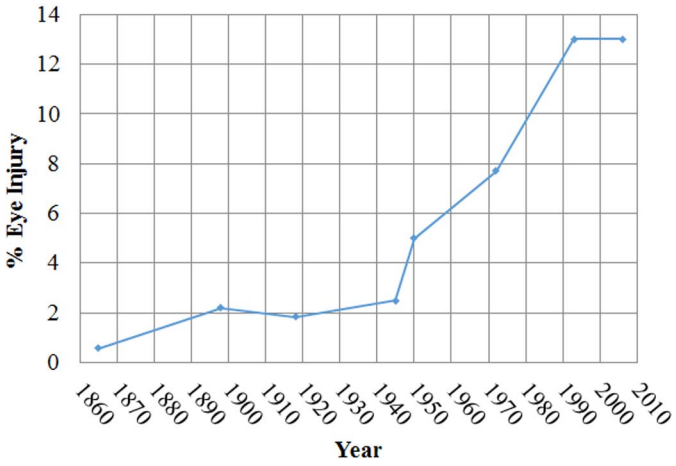

Figure 1. Percentage of eye injuries out of all combat injuries for US forces involved in major conflicts from 1865–2009.[1–5]

true. Understanding the mechanism of primary blast-induced ocular trauma is therefore very important to understanding the pathogenesis of blast-related eye injuries.

Computational models of ocular trauma have traditionally focused on blunt trauma[8–13] though some recent models have studied the effects of primary blast.[14,15] It should be noted that all existing computational models of ocular injury to this point have exclusively modeled the human eye while nearly all experimental models use porcine eyes. Some of these studies have used physical data from concurrent impact experiments,[11,12] while others were based on experimental data reported by other researchers.[13,16] No primary blast data is currently available for the validation of blast models, though we have recently shown significant ocular damage can arise from primary blast exposure.[17] These computational impact studies have reported the response of the eye in terms of the deflection under impact, parameters for prediction of globe rupture, and intraocular pressure (IOP) to correlate the model predictions with experimental data.

We previously performed shock tube experiments on porcine eyes and described damage arising from exposure to sublethal levels of primary blast.[17] The location and severity of ocular damage was recorded. In the present study, we developed the first whole-eye model of the porcine eye. This model was subjected to simulated blast loading to give insights into the mechanisms of the experimentally-observed damage. This model was validated using previously-published impact data because appropriate blast data were not available. The model's predictions correlated strongly with our previous findings of blast-exposed porcine eyes.

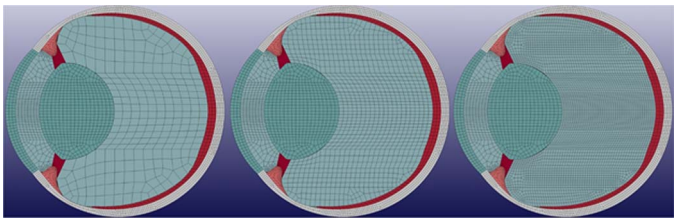

Figure 2. Cross-sectional view through the optical axis of the modeled porcine eye. The assembled eye model was meshed with three different characteristic hexahedral element length scales: 1 mm (*left*), 0.5 mm (*center*), and 0.25 mm (*right*).

Methods

Anatomy and Geometry

Geometry for a Finite Element Analysis (FEA) model of a porcine eye was created in three dimensions using SolidWorks (Dassault Systèmes SOLIDWORKS Corp., Waltham, MA) in quarter symmetry with dimensional data taken from a variety of sources (Fig. 2; Table 1). The sclera was modeled with a continuously varying thickness ranging from 0.43 to 0.89 mm.[18] The globe's overall diameter in the coronal plane was 22.2 mm, and length in the transverse/sagittal planes was 22.9 mm. The zonules were simplified for computational purposes into a continuous band of material connecting the lens equator to the ciliary body. The ciliary body was also simplified, combining all the ciliary muscles and connective tissues into one contiguous and homogeneous material. The iris was not modeled to reduce computational complexity of the model. The retina and choroid were modeled as a single layer with thickness equal to that of both tissue layers combined. This was done to avoid the computational expense of the very small elements required for the thin cross sections of the retina and choroid. The optic nerve head and optic nerve were not modeled for the same reason. The aqueous and vitreous geometry resulted from the anterior and posterior chamber geometry defined by the previously described components.

Mesh, Model Construction, and Boundary Conditions

Each "part" (i.e., tissue or collection of tissues) was meshed using CUBIT (Sandia National Laboratories, Albuquerque, NM) meshing software. Each part was

Table 1. Dimensions and Sources for Porcine Eye Model

Geometry	Dimensional Value (mm)	Source
Scleral outer radius	11.12 mm (calculated to match area value)	18
Scleral inner radii	Various (see text)	18
Corneal outer radius	9.01 mm	28
Corneal thickness	0.98 mm at apex	29
Lens anterior radius	6.63 mm	28
Lens posterior radius	5.08 mm	28
Lens equator position	2.5-mm posterior to posterior surface of cornea	28
Zonules	Simplified for simulation purposes	30, 31
Ciliary body	Simplified for simulation purposes	Histology
Iris root thickness	N/A	31
Iris collarette thickness	N/A	31
Pupil diameter	N/A	31
Chorioretina thickness	Continuous variation from 0.2–0.86 mm	31, 32

cut into meshable volumes, imprinted to ensure mesh coherence at the cut junctions, and meshed using hexahedral elements with a maximum element size of 1 mm in the interest of accurately propagating shock waves.[19] The meshed model is shown in Figure 2.

Meshed parts were then imported into LS-DYNA (LSTC, Livermore, CA) following assembly using LSPREPOST (LSTC). Contacts were defined for each part-to-part contact as follows. The lens to zonules, zonules to ciliary body, ciliary body to sclera, and sclera to cornea were attached sequentially. This contact type ties the nodes and outer segments of the two parts together at the contact interface so that the displacements of adjacent tissues must be equal. Failure of the contact was not modeled at these attachments. Contacts between the vitreous and all other structures, retina and all other structures, and aqueous and all other structures were modeled allowing a failure criterion to be defined at the contact junction. Due to a lack of knowledge of the specific failure thresholds for these junctions in the physical eye, the failure values were set to a level thought to be above reported physiological failure levels of the tissues, with the exception of the retina-to-sclera junction; this contact interface was varied experimentally to obtain a failure level that corresponded to retinal detachments observed in concurrent physical experiments.[17] Liu et al.[16] used a value of 340 ± 78 Pa for the retinal adhesive force; this value was used as the initial value in the present model. The eye was modeled in a rigid holder filled with gelatin, mimicking the experimental setup.[17] Rigid boundary conditions and material were used for the holder. The gelatin contact with the holder was tied. Contact between the gelatin and sclera was specified with translation allowed between the surfaces to simulate potential slippage between the two parts.

Blast loading was applied to the exposed forward facing surfaces of the eye and gelatin. Static overpressure-time history recorded in the physical experiments was used.[17] Three cases were represented and defined as peak overpressures of 0.05, 0.1, and 0.15 MPa. The three blast profiles are shown in Figure 3. The model contains 64,460 elements.

Material Models and Properties

Preliminary computational results indicated that the properties of the cornea and sclera dominated the response of the model. Uchio et al.[10] found that the elastic modulus of these materials decreased near the failure point. Bisplinghoff et al.[20] found an essentially linear stress-strain relationship at high loading rates. In the region far below failure the available stress-strain data for cornea and sclera is linear, regardless of the value or methodology used to obtain it. Tests of the model with various types of constitutive models for cornea and sclera found little difference in response, with the dominant variable always the stiffness of the tissue. Linear elastic models were therefore chosen to represent the cornea and sclera. The stiffness of the cornea and sclera was iterated from starting values based on the work of Rossi et al.[13] Final values were chosen based on matching the experimental data of the Delori BB impact experiment[21] and are shown in Table 2.

The aqueous humor was modeled using a linear

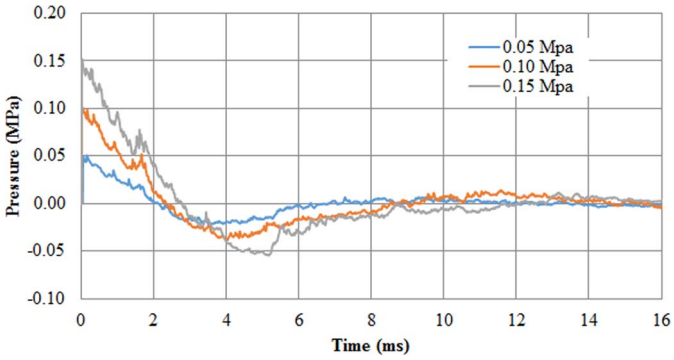

Figure 3. Overpressure-time histories from physical experiments using the shock tube.[17] These were selected as representative for three levels of blast and applied as a boundary condition in the present model. Legend entries correspond to the peak overpressure for each waveform.

fluid model available in LS-DYNA. The aqueous is compositionally similar to a saline solution and therefore is not expected to exhibit complex rheological behavior. The vitreous humor was modeled with a viscoelastic model using properties described by Rossi et al.[13]

The remaining tissues, chorioretina, zonules, ciliary body, and lens, were modeled as linear elastic with values taken from various sources in the literature as indicated in Table 2.

The compressibility of the chorioretina was found to have a significant effect on the model under blast loading. Sigal et al.[22] reported Poisson's ratio in the range of 0.40 to 0.49. A value of 0.47 (i.e., slightly compressible) was used since preliminary simulations showed that the model exhibited more overall deformation and significant compression of the chorioretina. With a Poisson's ratio of 0.49 (i.e., largely incompressible), the chorioretina exhibited significantly less deformation than with the 0.47 (largely compressible) and for that reason results are included from simulations using both values. Hereafter, simulations performed using a Poisson's ratio of 0.47 will be referred to as the compressible model while those with a value of 0.49 will be referred to as the incompressible model.

Mesh Sensitivity Analysis

A mesh sensitivity study was performed to determine the mesh density required to achieve computational accuracy. Panzer et al.[19] suggested that blast simulations should be conducted using hexahedral elements with characteristic lengths of 1 mm or less. Meshes were therefore created with characteristic element sizes of 1, 0.5, and 0.25 mm. The compressible retina model exposed to the 0.15 MPa blast level shown in Fig. 3 was used for the convergence study as it exhibited larger deformations and would therefore require a finer mesh to achieve convergence. Three metrics were selected for the evaluation of mesh convergence: (1) corneal apex displacement, (2) pressure at the center of the vitreous, and (3) stress at the macular area of the retina.

A grid convergence index (GCI) assessment was performed for peak values of the corneal apex displacement, vitreous pressure, and pressure at the macula.[23,24] The GCI method gives the rate of convergence of the solution as mesh size decreases and predicts the range of error in which the exact solution falls within 95% confidence intervals. This methodology is especially useful for cases such as this where the exact solution is not known. It should be noted that GCI predicts the exact solution of the ideal

Table 2. Material Property Definitions

Part Name	Density g/mm^3	Young's Modulus MPa	Bulk Modulus MPa	Poisson's Ratio	Source
Aqueous	0.0010	–	2200	–	33
Choroid	0.0010	0.05	–	0.47	22
Ciliary	0.0016	11	–	0.45	9
Cornea	0.0014	12	–	0.487	13
Gelatin	0.0010	–	2260	–	9
Lens	0.0011	1.5	–	0.499	12
Retina	0.0010	0.05	–	0.47	22
Sclera	0.0014	28	–	0.49	13
Vitreous	0.0010	–	2000	–	33
Zonules	0.0010	5	–	0.45	12

mesh size of the model; it does not account for material properties, material models, geometry, or the many other variables possible in a FEA model. The same three metrics were also evaluated over a time history using the relative error in L_2 norm. The L_2 norm is sensitive to small fluctuations in the data if they happen to be out of phase. The nature of the data in this experiment includes high frequency noise in some measurements and the relative error between different mesh sizes can be moderate, while the overall shape of the curve is fairly well matched. The 0.25-mm mesh was used as the baseline for this analysis.

Model Verification and Validation

Ideally, dynamic deformation data would be extracted from high-speed videos of blast experiments for validation; however, no such data is currently available. Therefore, validation of the model was performed against projectile impact studies in which porcine eyes were impacted with BBs.[21] BB impact was chosen as the worst case scenario for validation as it induces large localized strains at very high strain rates. These experiments were designed to inflict maximum deformation without inducing open-globe injury.

The experimental impact setup was duplicated as closely as possible within the modeling environment. The reported dimensions of the gelatin used to mount the eye were used, as were viscoelastic properties of the 10% gelatin used to pot the eyes.[25] A 4.5-mm diameter, 0.345-gram BB impacted the center of the cornea at a velocity of 62.3 m/s. Indentation of the cornea, equatorial variation, and longitudinal variation of the globe were measured versus time and compared with the data reported by Delori.[21]

Finally, the response of the model was also compared to that of other computational models and locations of maximum stresses and strains compared with the locations of primary blast-induced damage in the ex vivo porcine eyes.[17]

The ability of the finite element model to predict blast effects was found to depend on the element mesh size, presumably due to the relative stiffness and wave propagation accuracies of the various mesh densities. The FEA solutions were found to be largely independent of mesh density for meshes with characteristic element sizes of 0.5 mm and smaller (Fig. 4B). The GCI and L_2 norms were largely unchanged for all responses once the characteristic element size was reduced to 0.5 mm (Table 3). Therefore, the 0.5-mm mesh was deemed sufficiently dense to reproduce the key features of both primary blast and blunt impact in the porcine eye model. All subsequent results are reported based on this mesh. Simulation of the first 2 ms of the 0.15 MPa blast using the 0.5-mm mesh required 12 hours using 96 cores on a cluster computer.

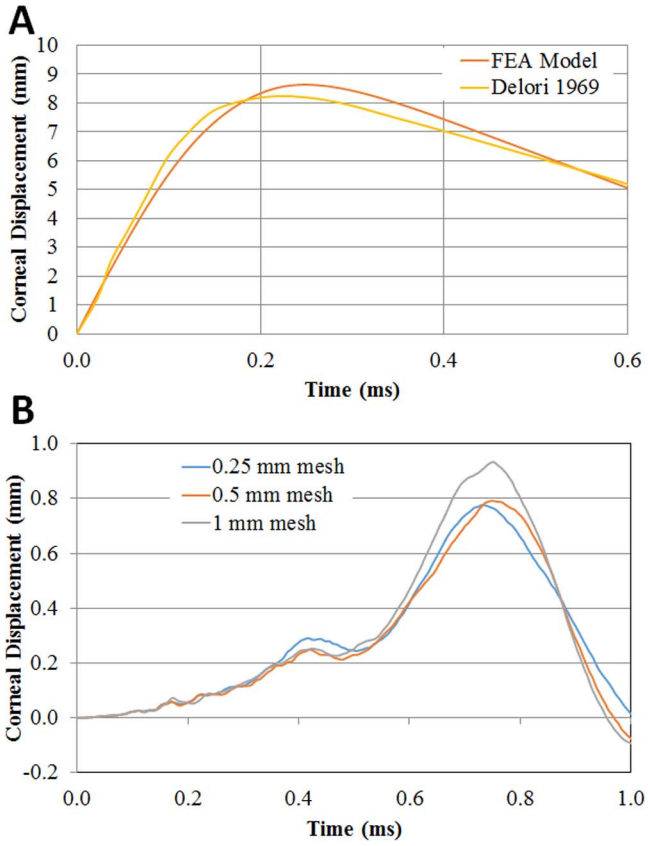

Figure 4. (A) Corneal displacement-time history for simulation of BB impact compared to the data of Delori. (B) Corneal displacement-time history for simulation of blast exposure for the three characteristic mesh sizes. Increasing mesh density beyond a characteristic element length scale of 0.5 mm did not significantly alter the time course of the predicted deformations.

Results

Manipulation of scleral and corneal stiffness parameters allowed substantial agreement between the model's predicted corneal displacement during BB impact and the data reported by Delori (Fig. 4A).[21] A video of this impact simulation is included in the supplemental data (Video S1).

Measurements of corneal apex displacement, pressure near the center of the vitreous, stress at the anterior and posterior surface of the ciliary body, stress and compression at the macula of the retina, and stress in the sclera increased with higher levels of

Table 3. Results of the Mesh Convergence Study

		Peak Values for Each Mesh				Convergence		% Error*	
Response	Units	1 mm	0.5 mm	0.25 mm	Asymptotic	Rate	GCI	1 mm	0.5 mm
Corneal Displacement	mm	0.933	0.792	0.776	0.767	1.48	0.014	19.7	10.8
Vitreous pressure	kPa	145	149	150	151	0.97	0.010	12.5	11.5
Retina stress	kPa	26.5	27.6	28.4	29.8	0.66	0.061	12.0	10.3

* Error in L_2 norm relative to 0.25-mm mesh

blast overpressure (Fig. 5). These metrics were selected to allow correlation with observable tissue responses from physical experiments of primary blast exposure in porcine eyes. Corneal apex displacement can be visually observed using high speed videos of blast exposures.[17] Pressure in the vitreous has been measured in at least one blast study and many blunt trauma studies.[12,26] Stress in the ciliary body was of interest due to the number of angle injuries observed in the blast experiments.[17] Scleral and retinal measurements of stress were also performed due to commonly observed damage in these regions during physical experiments. In the compressible retina model, all stress and displacement measures were lower than those for the incompressible retina model at all levels of blast. For pressure measurements this was reversed, with the less compressible model displaying higher pressure in the vitreous. Increasing the chorioretinal Poisson ratio from 0.47 to 0.49 resulted in an increase in vitreous pressure at all blast energies (Fig. 5B) but a decrease in all other peak responses, often by approximately 50%.

Locations of peak stresses (Fig. 6A) were highly coincidental with common locations of damage in blast experiments.[17] The motion of the vitreous relative to the ciliary body induces shearing at the junction between the ciliary body and sclera (Fig. 6B). Maximum stresses in the ciliary muscle are perpendicular to this interface, potentially indicating a mechanism for angle recessions and cyclodialysis observed in physical experiments reported by Sherwood et al.[17] (Fig. 6C).

Discussion

In our previous experimental work,[17] primary blast-induced ocular damage was most often seen in the sclera, angle, retina, choroid, and optic nerve head. Damage to the angle indicated a coup mechanism in which the ciliary body was detached from the sclera starting at the angle due to the blast-induced inertia imparted on the lens and vitreous. Posterior segment damage was probably due to contrecoup effects. In an effort to better understand the mechanisms underlying these results, we constructed a finite element model of the porcine eye. The eye model was then exposed (numerically) to the same overpressure-time profiles used in the shock tube experiments.

This model fills the current disconnect between experiments and simulations: the experimental study of ocular trauma is conducted almost exclusively using the porcine eye, whereas all prior computational models represent the human eye. While similar, significant differences exist in both the anatomy and mechanical properties of these eyes.

The response of the model to the blast was initial longitudinal compression and rearward displacement with equatorial expansion. The compression chiefly involved the anterior chamber, lens, and vitreous moving rearward while the posterior sclera remained largely in place. Following maximum compression, the model rebounded back toward its original shape while undergoing complex oscillations. Using the full positive and negative phase of the blast data, the model would avulse from the gelatin. Complete avulsion of the eye from the gelatin was observed in a number of our shock tube experiments at the 0.15-MPa blast level.[17] Internally, the individual components of the model oscillated at different frequencies according to mass and stiffness. Overall displacement of the cornea at the highest level of blast, 0.15 MPa, was on the order of 1 mm, in agreement with high speed video of the physical blast experiments.

The model showed increased levels of stress in areas of injury found in the physical experiments[17] (Fig. 6A). The highest levels of stress were found in the sclera in the region of the vitreous base (Fig. 6B). These values ranged up to 1 MPa, and were approximately 75% higher for the compressible retina model than the incompressible model. The peak stress in this area was coincident in time with the initial compression phase of the eyeball over the first 1 ms of the simulation. The

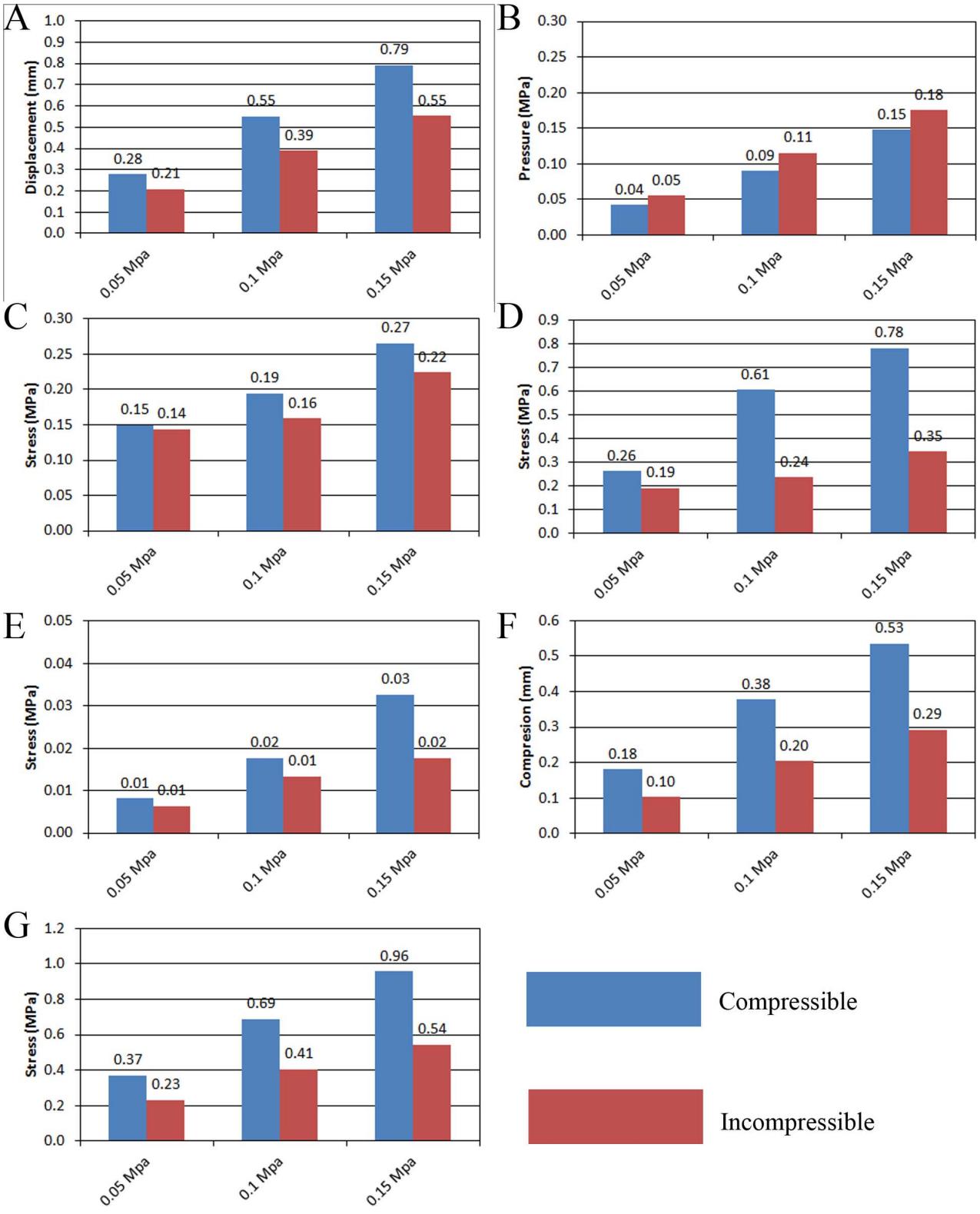

Figure 5. Maximum responses for each of the three pressure-time histories given in Figure 3 for models having compressible ($\nu = 0.47$) and incompressible ($\nu = 0.49$) retinae. (A) Posterior displacement of the corneal apex. (B) Pressure within the central vitreous. (C) Stress within the anterior ciliary body. (D) Maximum stress arising within the posterior ciliary body. (E) Maximum stress arising in the peripapillary retina. (F) Greatest extent of compression in the peripapillary retina. (G) Maximum stress within the sclera at the vitreous base.

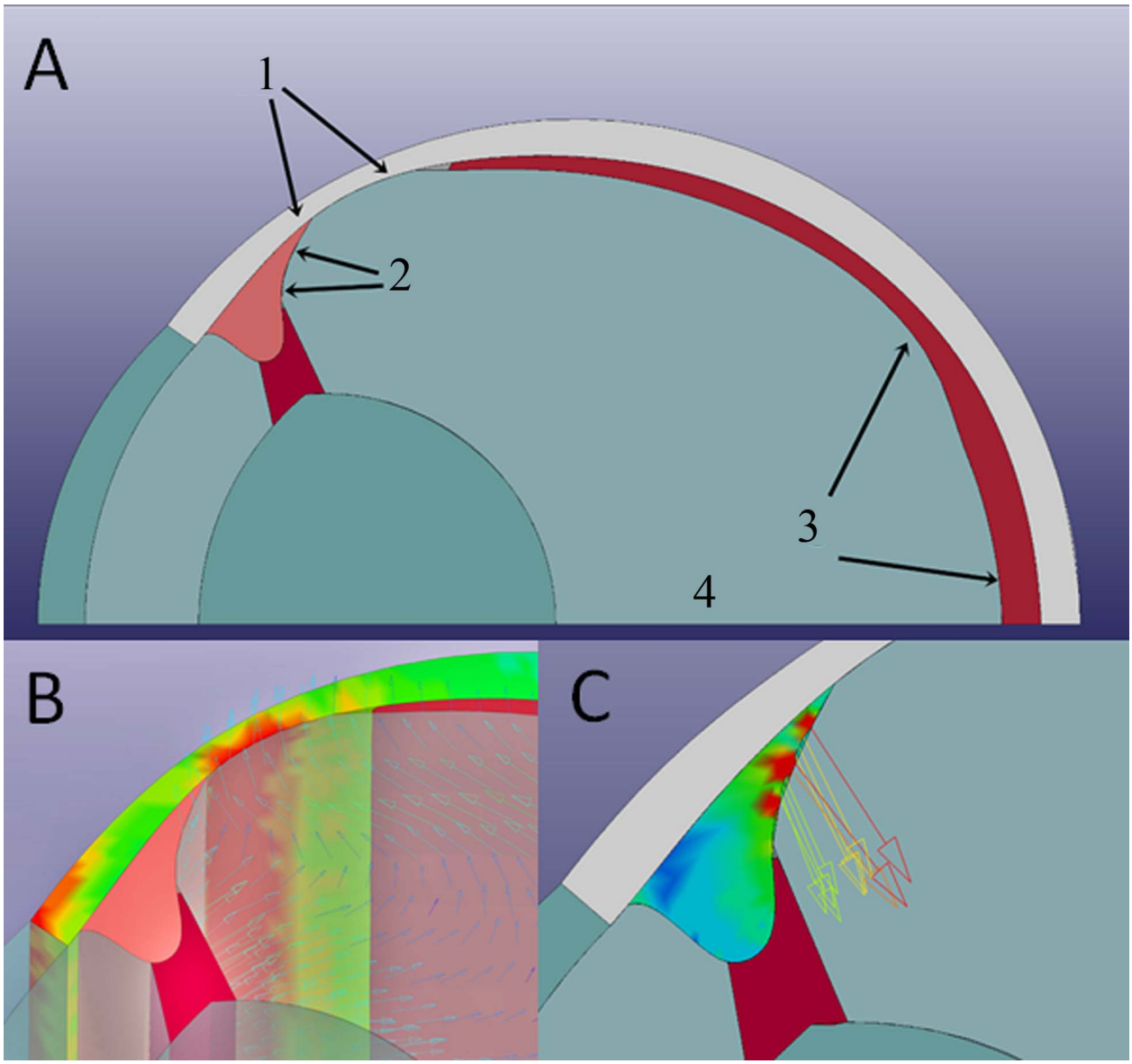

Figure 6. (A) Areas of peak stress in sclera (1), ciliary body (2), and retina (3), with location of pressure measurement in the central vitreous (4). (B) Peak stress in sclera at vitreous base (*red*). *Arrows* show instantaneous direction of vitreous movement. (C) Peak stress at posterior surface of ciliary body (*red*). *Arrows* show instantaneous movement of vitreous attached to ciliary body.

areas of maximum stress were found in the thinnest section of the sclera, adjacent to the vitreous base, centered longitudinally at the vitreous base attachment (Fig. 6B). This section of the sclera acts as a hinge between the anterior and posterior chambers, which displayed relative differential movement in the model. The attachment of the relatively massive vitreous places additional stress on this area as it resonates out of phase with the movement of the sclera. The stress concentration in this area correlated well with the equatorial location of scleral delamination observed in the physical experiments.

The next highest levels of stress were found in the ciliary body at its posterior surface, ranging up to 0.8 MPa (Fig. 6C). The stress in this region was induced by differential movement with the attached vitreous, occurring later in time compared with the nearby stress in the sclera, coincident with the initial rebound of the anterior chamber following its rearward displacement at the onset of the blast wave. Again, the level of regional stress was decreased in the incompressible retina model. The anterior surface of the ciliary body returned stress levels up to 0.27 MPa.

Angle recession and cyclodialysis were the most

common findings in the physical experiments. The model suggests a possible mechanism for these injuries as the ciliary muscles are pulled on by the vitreous from behind at the same time the anterior portion of the sclera to which the ciliary muscles are attached rebounds forward. This finding merits follow on work with a more detailed description of the individual ciliary muscles and zonules. Material property testing of the ciliary muscles and their adhesion to the vitreous and sclera would benefit this effort.

Rearward displacement of the vitreous compressed the retina between the vitreous and the sclera. This compression occurred with both the compressible and incompressible retina material properties. The maximum compression of the retina predicted by the compressible model was a 62% decrease in thickness at the retinal apex, with 33% compression in the incompressible retina model. For the highest level of blast, peak pressure on the retina was 0.36 MPa in the incompressible model and 0.30 MPa for the compressible model. Stress levels in the retina were an order of magnitude lower than the pressure, 0.02 to 0.03 MPa. Chorioretinal detachments were among the most common types of damage observed by Sherwood et al.[17] The model indicates a coup-contrecoup mechanism of injury to the retina due to the movement of the vitreous. The findings on retinal dynamics merit further work with more detail. It is known that the retina is nonhomogenous, with blood vessels throughout its structure. Histopathology suggests that the junction between the different material properties of the retina and blood vessel is susceptible to the initiation of a retinal detachment. The optic nerve head presents the same type of discontinuity, along with the tethering effect of the optic nerve. Though modeling these very thin tissues would be computationally intensive it may be possible to create smaller submodels based on the overall loading conditions determined with the present whole-eye model.

Only the model proposed by Rossi et al.,[13] which was validated using a blunt impact experiment, has been used to investigate blast effects on a detailed whole-eye model.[14,15] Blunt impact was used to validate the model because no blast loading data were available. Small changes were made to material properties and the model was placed in an Eulerian domain to incorporate primary blast loading ranging from sublethal to levels corresponding to 50% survivability for humans. These studies concluded that pressure levels at the macula could explain optic nerve and retina damage in blast survivors.

Dynamic FEA models of soft tissue structures are subject to certain limitations. The primary limitation is the lack of material properties derived specifically for use in a computational model intended to simulate high loading rates. Though the material models are capable of simulating rate effects and anisotropy, few tissues are characterized this way, particularly for the extremely rapid loading imposed by blast. Care was taken to ensure the model had a coherent response when compared to physical experiments; however, the addition of more detailed and specific material properties would significantly improve the model. Secondarily, the eye contains many small structures such as the zonules, blood vessels, iris, lamina cribrosa, and so on. These structures are of interest when characterizing certain injuries. However, modeling them with FEA as part of a larger overall model of the eye would require extremely fine mesh, leading to a very computationally expensive model. Finally the internal contacts between tissues in the eye have not been characterized and are therefore not well defined in the FEA model. The connection between the vitreous and retina in particular is not well quantified. The dynamics of the model in this work show that any connection between the vitreous and retina would induce traction force on the retina, contributing to retinal detachments, which have been observed experimentally.[17]

Additional simulations for longer times included the negative phase of the blast. In these cases, the eye was avulsed from the gelatin. While avulsion did occur in several of the physical blast experiments at higher levels of overpressure,[17] it did not occur in all cases. This may indicate the need for an improved boundary condition between the gelatin and the sclera. It may be possible to estimate the adhesion forces bonding the two via experiments but thus far no such data are available. Still, this finding indicates that the negative phase of primary blast could significantly strain the extraocular muscles and optic nerve.[17,34,35]

The orbital geometry used in the present simulations was simplified to mimic the experimental geometry used by Sherwood et al.[17] This is not a rigorous recreation of the human orbital anatomy and may result in differences between modeling predictions and the true ocular response to primary blast.[27] Future studies will attempt to address the importance of this issue by placing a human eye model in a more realistic human orbital geometry and repeating these simulations. This was not done in the present study as we were trying to replicate our own blast experiments as closely as possible.

The encouraging results correlating stress concentrations in the model with areas of injury in the physical experiments show that additional work could have many benefits. The current study specifically modeled the porcine eye. A model of the human eye constructed using the same methodologies would provide a useful basis of comparison between porcine eyes, which are more easily obtained for experiments, and human eyes. A series of experiments on porcine eyes to determine loading rate-dependent material properties specifically for use in the FEA model would improve the fidelity of the present porcine model. Smaller submodels of detailed structures such as the optic disc, ciliary body, anterior chamber, and zonules could be constructed using larger overall boundary conditions from the basic model of the eye, with the ultimate goal of constructing a detailed overall model incorporating all of these elements for comparison and validation with future physical experiments. The incorporation of more advanced material models will significantly improve the model predictions of traumatic events. Unfortunately, no suitable data for calibrating such models is currently available.

Acknowledgments

The authors thank the UTSA Department of Mechanical Engineering for allowing the use of significant computational resources in support of this project.

Supported by the U.S. Army Medical Research and Material Command under Vision Research Program Grant Number W81XWH-12-2-0055. The opinions or assertions contained herein are the private views of the authors and are not to be construed as official views of the Department of the Army of the Department of Defense.

Disclosures: **R. Watson,** None; **W. Gray,** None; **W.E. Sponsel,** None; **B.J. Lund,** None; **R.D. Glickman,** None; **S.L. Groth,** None; **M.A. Reilly,** None

References

1. Ari AB. Eye injuries on the battlefields of Iraq and Afghanistan: public health implications. *Optometry*. 2006;77:329–339.
2. Breeze J, Allanson-Bailey LS, Hunt NC, et al. Surface wound mapping of battlefield oculofacial injury. *Injury*. 2012;43:1856–1860.
3. Mader TH, Carroll RD, Slade CS, George RK, Ritchey JP, Neville SP. Ocular war injuries of the Iraqi Insurgency, January-September 2004. *Ophthalmology*. 2006;113:97–104.
4. Thach AB, Johnson AJ, Carroll RB, et al. Severe eye injuries in the war in Iraq, 2003-2005. *Ophthalmology*. 2008;115:377–382.
5. Weichel ED, Colyer MH, Ludlow SE, Bower KS, Eiseman AS. Combat ocular trauma visual outcomes during Operations Iraqi and Enduring Freedom. *Ophthalmology*. 2008;115:2235–2245.
6. Scott R. The injured eye. *Philos Trans R Soc Lond B Biol Sci*. 2011;366:251–260.
7. Abbotts R, Harrison SE, Cooper GL. Primary blast injuries to the eye: a review of the evidence. *J R Army Med Corps*. 2007;153:119–123.
8. Cirovic S, Bhola RM, Hose DR, et al. Computer modelling study of the mechanism of optic nerve injury in blunt trauma. *Br J Ophthalmol*. 2006;90:778–783.
9. Power ED. *A nonlinear finite element model of the human eye to investigate ocular injuries from night vision goggles. Mechanical Engineering*. Blacksburg, VA: Virginia Polytechnic Institute and State University; 2001. Thesis.
10. Uchio E, Ohno S, Kudoh J, Aoki K, Kisielewicz LT. Simulation model of an eyeball based on finite element analysis on a supercomputer. *Br J Ophthalmol*. 1999;83:1106–1111.
11. Gray W, Sponsel WE, Scribbick FW, et al. Numerical modeling of paintball impact ocular trauma: identification of progressive injury mechanisms. *Invest Ophthalmol Vis Sci*. 2011;52:7506–7513.
12. Stitzel JD, Duma SM, Cormier JM, Herring IP. A nonlinear finite element model of the eye with experimental validation for the prediction of globe rupture. *Stapp Car Crash J*. 2002;46:81–102.
13. Rossi T, Boccassini B, Esposito L, et al. The pathogenesis of retinal damage in blunt eye trauma: finite element modeling. *Invest Ophthalmol Vis Sci*. 2011;52:3994–4002.
14. Rossi T, Boccassini B, Esposito L, et al. Primary blast injury to the eye and orbit: finite element modeling. *Invest Ophthalmol Vis Sci*. 2012;53:8057–8066.
15. Esposito L, Clemente C, Bonora N, Rossi T. Modelling human eye under blast loading. *Comput Methods Biomech Biomed Engin*. 2015;18:107–115.

16. Liu X, Wang L, Wang C, Sun G, Liu S, Fan Y. Mechanism of traumatic retinal detachment in blunt impact: a finite element study. *J Biomech*. 2013;46:1321–1327.
17. Sherwood D, Sponsel WE, Lund BJ, et al. Anatomical manifestations of primary blast ocular trauma observed in a postmortem porcine model. *Invest Ophthalmol Vis Sci*. 2014;55:1124–1134.
18. Olsen TW, Sanderson S, Feng X, Hubbard WC. Porcine sclera: thickness and surface area. *Invest Ophthalmol Vis Sci*. 2002;43:2529–2532.
19. Panzer MB, Myers BS, Bass CR. Mesh considerations for finite element blast modelling in biomechanics. *Comput Methods Biomech Biomed Engin*. 2013;16:612–621.
20. Bisplinghoff JA, McNally C, Manoogian SJ, Duma SM. Dynamic material properties of the human sclera. *J Biomech*. 2009;42:1493–1497.
21. Delori F, Pomerantzeff O, Cox MS. Deformation of the globe under high-speed impact: it relation to contusion injuries. *Invest Ophthalmol*. 1969;8:290–301.
22. Sigal IA, Flanagan JG, Ethier CR. Factors influencing optic nerve head biomechanics. *Invest Ophthalmol Vis Sci*. 2005;46:4189–4199.
23. Roache PJ. A method for uniform reporting of grid refinement studies. *J Fluids Eng*. 1994;116:405–413.
24. Schwer LE. Is your mesh refined enough? Estimating discretization error using GCI. LS-DYNA User Forum, Bamberg, Germany; 2008.
25. Parker NG, Povey MJW. Ultrasonic study of the gelation of gelatin: phase diagram, hysteresis and kinetics. *Food Hydrocoll*. 26:99–107.
26. Alphonse VD. *Injury Biomechanics of the Human Eye During Blunt and Blast Loading*. *Biomedical Engineering*. Blacksburg, VA: Virginia Polytechnic Institute and State University; 2012. Thesis.
27. Bhardwaj R, Ziegler K, Seo JH, Ramesh KT, Nguyen TD. A computational model of blast loading on the human eye. *Biomech Model Mechanobiol* 2014;13:123–140.
28. Reilly MA, Hamilton PD, Perry G, Ravi N. Comparison of the behavior of natural and refilled porcine lenses in a robotic lens stretcher. *Exp Eye Res* 2009;88:483–494.
29. Asejczyk-Widlicka M, Schachar RA, Pierscionek BK. Optical coherence tomography measurements of the fresh porcine eye and response of the outer coats of the eye to volume increase. *J Biomed Optics* 2008;13:024002.
30. Burd HJ, Judge SJ, Cross JA. Numerical modelling of the accommodating lens. *Vision Res* 2002;42:2235–2251.
31. Bron AJ, Tripathi RC, Tripathi BJ. *Wolff's Anatomy of the Eye and Orbit*. *8th ed*. London: Hodder Arnold Publishers; 1997.
32. Sanchez I, Martin R, Ussa F, Fernandez-Bueno I. The parameters of the porcine eyeball. *Graefes Arch Clin Exp Ophthalmol*. 2011;249:475–482.
33. Reiss S, Burau G, Stachs O, Guthoff R, Stolz H. Spatially resolved Brillouin spectroscopy to determine the rheological properties of the eye lens. *Biomed Optics Exp*. 2011;2:2144–2159.
34. Sponsel WE, Gray W, Groth SL, Stern AR, Walker JD. Paintball trauma and mechanisms of optic nerve injury: rotational avulsion and rebound evulsion. *Invest Ophthalmol Vis Sci*. 2011;52:9624–9628.
35. Asemota BL, Glickman RD, Rodriguez L, Sponsel WE, Reilly MA. Torsional indirect traumatic optic neuropathy (TITON): a physiologically relevant animal model of traumatic optic neuropathy. *Invest Ophthalmol Vis Sci*. Submitted.